

Rethinking Fine-Tuning: Unlocking Hidden Capabilities in Vision-Language Models

Mingyuan Zhang¹ Yue Bai¹ Yifan Wang¹ Yiyang Huang¹ Yun Fu^{1,2}

¹College of Engineering, Northeastern University

²Khoury College of Computer Science, Northeastern University

{zhang.mingyua, bai.yue, wang.yifan25, huang.yiyan, y.fu}@northeastern.edu

Abstract

Explorations in fine-tuning Vision-Language Models (VLMs), such as Low-Rank Adaptation (LoRA) from Parameter Efficient Fine-Tuning (PEFT), have made impressive progress. However, most approaches rely on explicit weight updates, overlooking the extensive representational structures already encoded in pre-trained models that remain underutilized. Recent works have demonstrated that Mask Fine-Tuning (MFT) can be a powerful and efficient post-training paradigm for language models. Instead of updating weights, MFT assigns learnable gating scores to each weight, allowing the model to reorganize its internal subnetworks for downstream task adaptation. In this paper, we rethink fine-tuning for VLMs from a structural reparameterization perspective grounded in MFT. We apply MFT to the language and projector components of VLMs with different language backbones and compare against strong PEFT baselines. Experiments show that MFT consistently surpasses LoRA variants and even full fine-tuning, achieving high performance without altering the frozen backbone. Our findings reveal that effective adaptation can emerge not only from updating weights but also from reestablishing connections among the model’s existing knowledge. Code available at: <https://github.com/MingK9/MFT-VLM>

1. Introduction

The advent of large-scale, pre-trained Vision-Language Models (VLMs) [30] represents a significant milestone in artificial intelligence [7]. By training on large-scale multimodal data, these models have demonstrated remarkable capabilities and set new state-of-the-art standards across a spectrum of tasks, including visual question answering (VQA) [1], image captioning, and complex multimodal reasoning [28]. The VLM ecosystem is expanding at an unprecedented rate, with the proliferation of powerful open-weight language models [4, 16, 50, 51, 68] built with fantastic vision back-

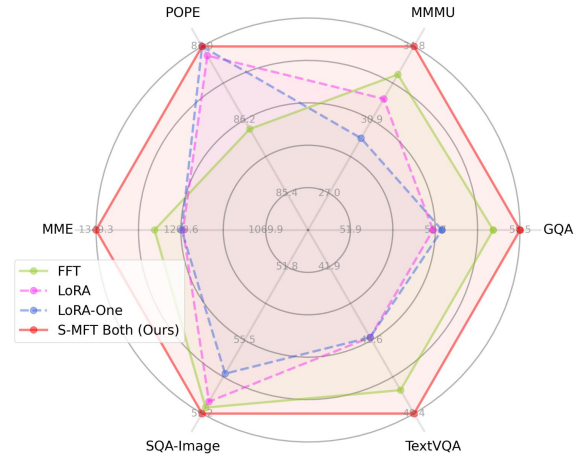


Figure 1. Overall performance comparison of different fine-tuning methods on VLM with Qwen2.5-0.5B as the language model. Our S-MFT consistently surpasses both FFT and LoRA-based approaches on all tasks. Among the variants, S-MFT Both achieves the strongest overall performance, highlighting the effectiveness of jointly masking both Attention and MLP layers.

bones [46, 59]. However, despite their impressive zero-shot generalization, these foundation models are inherently generalists. Achieving peak performance in specialized downstream applications, such as medical diagnostics [44], robotics [57], or domain-specific document understanding, requires task-specific adaptation.

Traditionally, Full Fine-Tuning (FFT) has been the default paradigm for this adaptation [9, 43]. However, as model-scale balloons into the hundreds of billions of parameters, FFT has become computationally and logically prohibitive, which demands massive computational resources and storage for each downstream task [61].

To address the limitations of FFT, Parameter-Efficient Fine-Tuning (PEFT) [61] methods have emerged as the standard fine-tuning methods for model adaptation. The core idea of PEFT is to freeze the vast majority of the pre-trained model’s parameters and update only a small, manageable

subset. Among the diverse PEFT techniques, Low-Rank Adaptation (LoRA) [21] has become the dominant paradigm. Instead of updating the massive pre-trained weights, LoRA injects two small, trainable low-rank matrices. This additive weight update philosophy governs most modern PEFT research [8, 23, 25, 32, 64, 65].

Although these methods have achieved remarkable success, they share a common assumption that effective adaptation requires modifying pre-trained weights. However, prior works show that pre-trained models contain transferable winning subnetworks that can be activated via masks to achieve satisfied performance [5, 13]. In this paper, we argue that such widely used fine-tuning methods overlook the latent representational richness, robust generalization, and inherent capability already encoded within pre-trained models.

Recent work introduced a new training paradigm called Mask Fine-Tuning (MFT), validating it as an effective and efficient post-fine-tuning method on Large Language Models (LLMs) that improves performance beyond the best FFT by learning a mask to remove redundant weight values [62]. This mechanism serves as a dynamic, learnable gating function that effectively reorganizes the model’s internal structure to better exploit and amplify the network’s capabilities. Following insight, we extend MFT into a general fine-tuning paradigm that starts directly from pre-trained models, enabling effective and efficient adaptation without updating original weights. Beyond the proven effectiveness of Hard Mask Fine-Tuning (H-MFT), we further propose Soft Mask Fine-Tuning (S-MFT), which allows the network greater flexibility to adapt and reorganize its internal structure through continuous, learnable masks.

We conduct extensive experiments applying MFT to the language and projector components of a diverse set of VLM backbones. The results demonstrate that MFT consistently and significantly surpasses strong PEFT baselines, including numerous LoRA variants. Remarkably, MFT’s performance can even exceed that of full fine-tuning while keeping the pre-trained model frozen. We summarize our contributions as follows:

- We extend H-MFT to S-MFT as novel paradigms and first apply them to fine-tune VLMs without updating any pre-trained weights.
- S-MFT consistently surpasses strong PEFT baselines (e.g., LoRA) and even outperforms FFT across multiple benchmarks with training efficiency when fine-tuning VLMs.
- We show that VLM adaptation can be reformulated as a continuous structural reparameterization process, where performance gains arise from reweighting and modulating pre-trained parameters rather than updating them.

2. Related Work

This work rethinks fine-tuning of VLMs as structural reparameterization rather than weight update. We contextual-

ize MFT within the broader landscape: 1) the evolution of fine-tuning methods for VLMs, 2) distinguishing MFT from model pruning, and 3) relevant mask-learning for fine-tuning methods of large pre-trained models.

2.1. Vision-Language Models Fine-tuning

FFT has been proven to be an effective transfer mechanism for downstream task adaptation of VLMs [42, 60]. However, the prohibitive costs of FFT have become a problem as model size scales up [61], leading to the rise of PEFT [61]. The vast majority of PEFT techniques, while diverse, operate on the shared assumption that adaptation requires introducing a weight update to the model. Adapter-Tuning [20] inserts small, bottleneck-shaped, and learnable neural modules (adapters) between the network layers. Prefix-Tuning [26] prepends a sequence of continuous and learnable vectors to the keys and values of the attention layers. Prompt-Tuning [24] simplifies Prefix-Tuning by adding learnable embeddings only to the input layer. P-Tuning [33] introduces a prompt encoder to optimize continuous prompts more stably. Low-Rank Adaptation (LoRA) [21] is based on the hypothesis that the update matrix has a low intrinsic rank. It freezes the pre-trained weights and injects a trainable low-rank branch. This additive weight update philosophy is shared by its many variants, such as DoRA [32], which decomposes the update into magnitude and direction components, and VeRA [23], which shares low-rank matrices across layers. In all these cases, adaptation is achieved by adding new parameters or updating weights. Instead, MFT adapts the model by learning masks and keeps the pre-trained weights frozen, operating on the antithetical premise that the knowledge is already present and needs to be unlocked.

2.2. Pruning and Latent Subnetworks

MFT shares conceptual connections with research on model pruning and latent subnetworks, which examine how over-parameterized models encode adaptable functional pathways. Neural network pruning [37, 41, 55] has been widely adopted across vision [11], language [35], and multimodal learning [36] for model compression [18, 22] and acceleration [10, 17, 39, 53, 54]. In parallel, the Lottery Ticket Hypothesis (LTH) [13] revealed that dense networks can contain sparse subnetworks capable of matching full-model performance. While, the Dual Lottery Ticket Hypothesis (DLTH) [5] further showed that even randomly selected subnetworks can be transformed into trainable ones through targeted regularization. Similar findings in pre-trained models such as BERT [34] indicate that transferable subnetworks exist and can be selectively activated for new tasks in large models, which is consistent with MFT’s view of reusing existing structures in foundation models within frozen weights. While both pruning and MFT involve identifying meaningful connections, their objectives diverge. Pruning focuses on

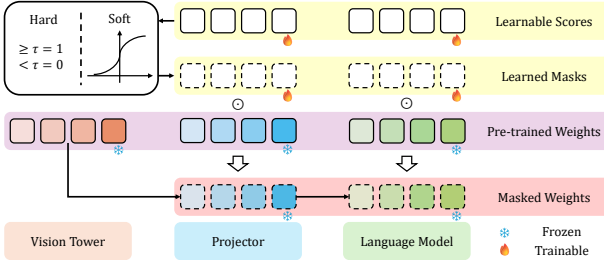


Figure 2. Overview of **Mask Fine-Tuning (MFT)** applied to a Vision-Language Model (VLM). The pre-trained parameters are all frozen during the training, while learnable scores are added to pre-trained weights in the projector and language model. We have two strategies to generate either hard or soft masks that modulate the effective weights.

efficiency by reducing model size and latency through sparsity [14, 48], which is often accompanied by a performance drop. In contrast, MFT leverages masking to reorganize and mask redundant parameters for adaptive knowledge expression and downstream performance gains.

2.3. Subnetwork and Mask Learning Adaptation

MFT belongs to a new and emerging class of methods focusing on subnetwork identification, in which adaptation is achieved solely by learning a mask over a completely frozen backbone. This paradigm reframes model adaptation as a structural selection problem rather than parameter optimization, aligning with a broader trend of identifying optimal subnetworks within pre-trained models [12, 19, 31, 49]. Early work, such as [66], demonstrates that binary masking of pre-trained weights in BERT and RoBERTa can achieve performance comparable to FFT while drastically reducing memory footprint. Regularized Mask Tuning (RMT) [67] extends this idea by optimizing masks on downstream tasks. However, RMT is applied to the vision encoder in CLIP [46] and learn task-specific masks. In contrast, MFT targets the language and projector components in VLMs, learns masks on a diverse, instruction-driven dataset, and is evaluated across multiple downstream tasks. Moreover, RMT uses only hard thresholding to learn binary masks, whereas we introduce continuous (soft) masks as an extension that enables more flexible gating and attenuation. [62] adopts a similar masking mechanism but operates as a post-fine-tuning enhancement on already well-fine-tuned models. Unlike these methods, MFT is a new general fine-tuning paradigm that replaces weight-based updates with learnable structural reparameterization, serving as an alternative to FFT and LoRA for large foundation models.

3. Mask Fine-Tuning (MFT)

We conduct Mask Fine-Tuning (MFT) approach for VLMs, specifically learning masks on the language model and pro-

jector components. The overview is shown in Fig. 2.

3.1. Mask Parameterization

For each pre-trained weight matrix $W \in \mathbb{R}^{m \times n}$ in the language model and projector, we introduce a learnable score matrix with the same size $S \in \mathbb{R}^{m \times n}$ to help generate the mask $M \in \mathbb{R}^{m \times n}$. The effective weight is computed as:

$$W' = W \odot M, \quad (1)$$

where \odot denotes element-wise multiplication, W is frozen during training.

3.2. Learnable Mask

We deploy MFT in two mask generation strategies with distinct training dynamics.

3.2.1. Binary (Hard) Mask

We follow the H-MFT method of [62]. For a target sparsity level $k \in [0, 1]$, we have the elements in the mask generated by the following:

$$M_{ij} = \begin{cases} 1, & \text{if } |S_{ij}| \geq \tau_k \\ 0, & \text{otherwise} \end{cases}, \quad i \in m, j \in n, \quad (2)$$

where τ_k is the k -th percentile of the sorted absolute scores $\{|S_{ij}|\}$, ensuring that exactly a fraction $(1 - k)$ of elements are retained. Formally, if we sort the scores as $|S_{(1)}| \geq |S_{(2)}| \geq \dots \geq |S_{(mn)}|$, then $\tau_k = |S_{(\lfloor k \cdot mn \rfloor)}|$, selecting the top- k fraction of weights by magnitude. We use the absolute values of the scores to ensure they are non-negative, which facilitates ranking.

Since this top- k selection operation is non-differentiable with zero or undefined gradients, we employ the Straight-Through Estimator (STE) [6] for gradient \mathcal{L} computation. The STE allows gradients to flow directly through the discrete masking operation by approximating the Jacobian as an identity mapping:

$$\frac{\partial M}{\partial S} \approx I, \quad (3)$$

where I denotes the identity. While the forward pass enforces strict binary values via top- k selection, the backward pass treats the operation as identity, enabling the scores S to receive meaningful gradient signals. By the chain rule:

$$\frac{\partial \mathcal{L}}{\partial S} = \frac{\partial \mathcal{L}}{\partial M} \cdot \frac{\partial M}{\partial S} \approx \frac{\partial \mathcal{L}}{\partial M} \cdot I = \frac{\partial \mathcal{L}}{\partial M}. \quad (4)$$

This approximation provides effective gradients for optimization, guiding which elements to mask or preserve.

3.2.2. Continuous (Soft) Mask

Although binary masking provides clear interpretability, its discrete nature can be overly restrictive, limiting the model’s representational flexibility and overall performance. To enable smooth optimization and avoid the gradient approximation bias in the hard mask learning, we introduce a differentiable alternative based on a sigmoid function that allows the model to smoothly learn sparsity patterns, automatically approaching an optimal sparsity level through training:

$$M_{ij} = \sigma\left(\frac{S_{ij}}{T}\right) = \frac{1}{1 + \exp(-S_{ij}/T)}, \quad (5)$$

where $T > 0$ is the temperature that controls the sharpness of the sigmoid function. Given an initialization value of scores S , we set T as small as possible to produce initial mask values close to 1, minimizing disruption to the pretrained model at the start of training. This strategy ensures that training begins from the pre-trained model’s original performance, allowing the optimization process to learn sparse patterns gradually. Notably, T cannot be too small, as an overly steep sigmoid would cause masks too close to 1, leading to vanishing gradients and preventing effective learning. We expect such a soft mask learning process to learn an adaptive tendency toward mask binarization.

While the sigmoid function is inherently differentiable, it enables direct gradient computation in soft mask learning. To ensure consistent comparison with the hard-mask approach, we also apply the straight-through estimator (STE) to the soft-mask method in our experiments.

3.3. Training Objective

MFT shares the exact objective function of FFT with learnable masks introduced:

$$\mathcal{L}(U_m) = \sum_i \log P(u_m^i | u_m^{i-k}, \dots, u_m^{i-1}; W \odot M), \quad (6)$$

where $U_m = \{u_m^1, \dots, u_m^n\}$ is the token sequence. We add the mask M on the given model parameters W , where M and W share the same size and the corresponding W is masked out by element-wise multiplication \odot .

3.4. Theoretical Guarantee

To verify the superiority of MFT’s optimization strategy over FFT, we follow the PAC-Bayes theory of generalization upper bounds [40], which has also been widely explored for neural networks [3], to provide theoretical insights from an information-theoretic perspective. Since our MFT uses the same training objective and dataset as FFT, the analysis is conducted under a fair-comparison scenario to compare the model’s generalization upper bound purely.

Given n as the size of the training set, δ as the degree of confidence, for any hypothesis h , which represents the

model here, we have the PAC-Bayes upper bound given by

$$\mathcal{L}(h) \leq \mathcal{L}_S(h) + \Phi(C(h)), \quad \Phi(u) = \sqrt{\frac{u + \ln \frac{1}{\delta}}{2(n-1)}}. \quad (7)$$

$\mathcal{L}(h)$ and $\mathcal{L}_S(h)$ represent training and test loss, respectively. $\Phi(C(h))$ is an additional complexity term to describe the model code length, where $C(\cdot)$ represents the encoding process. Then, we have

$$\begin{aligned} \mathcal{L}(h_{\text{FFT}}) &\leq \mathcal{L}_S(h_{\text{FFT}}) + \Phi(C_{\text{FFT}}) \\ \Rightarrow U(h_{\text{FFT}}) &= \mathcal{L}_S(h_{\text{FFT}}) + \Phi(C_{\text{FFT}}), \end{aligned} \quad (8)$$

$$\begin{aligned} \mathcal{L}(h_{\text{MFT}}) &\leq \mathcal{L}_S(h_{\text{MFT}}) + \Phi(C_{\text{MFT}}) \\ \Rightarrow U(h_{\text{MFT}}) &= \mathcal{L}_S(h_{\text{MFT}}) + \Phi(C_{\text{MFT}}), \end{aligned} \quad (9)$$

where $U(\cdot)$ means the loss upper bound of h . If we make a difference on two sides of Eq. 8 and Eq. 9, we have

$$\begin{aligned} U(h_{\text{MFT}}) - U(h_{\text{FFT}}) &= [\mathcal{L}_S(h_{\text{MFT}}) - \mathcal{L}_S(h_{\text{FFT}})] \\ &\quad + [\Phi(C_{\text{MFT}}) - \Phi(C_{\text{FFT}})], \end{aligned} \quad (10)$$

revised as

$$U(h_{\text{MFT}}) - U(h_{\text{FFT}}) = \Delta_{\text{train}} + \Delta_{\text{complexity}}. \quad (11)$$

For our case, to theoretically support that our MFT has better optimization potential than FFT, we need to verify that $\Delta_{\text{train}} + \Delta_{\text{complexity}} < 0$. Due to limited space, details are left in the Supplementary.

4. Experiments

We apply our Mask Fine-tuning (MFT) method on Vision-Language Models (VLMs) across different vision and language backbones and evaluate on diverse vision-language tasks. We also provide ablation studies and analyses from various perspectives to gain deeper insights into our method.

4.1. Experiments Setup

Vision Encoders. We follow the mainstream VLM training paradigm that keeps the vision encoder frozen and trains the projector and language model [30, 69]. Accordingly, all our main experiments adopt SigLIP [59] as the vision encoder to ensure consistency. We also conduct a small-scale comparison using CLIP [46] to verify the generality of MFT.

Language Model Backbones. We primarily explore and validate MFT on four compact language backbones, including Qwen2.5-0.5B [45], TinyLLaMA-1.1B [63], Gemma-2B [50], and Phi-2-2.7B [16], to demonstrate its effectiveness across diverse architectures. In addition, we conduct scale-up experiments on larger models to verify the feasibility and scalability of MFT as the model size increases.

Table 1. Main experimental result comparison with the average time cost of our proposed Soft Mask Fine-Tuning (S-MFT) with Full Fine-Tuning (FFT) and representative Parameter-Efficient Fine-Tuning (PEFT) baselines across four language backbones. **Red numbers** denote the best results, and **blue numbers** denote the second-best. S-MFT consistently achieves comparable or superior performance, with faster convergence, to both PEFT methods and FFT, demonstrating strong generality and efficiency across architectures.

Method	Evaluation Tasks						Epoch ↓	Time (h) ↓
	GQA ↑	MMMU ↑	POPE ↑	MME ↑	SQA-Image ↑	TextVQA ↑		
Qwen2.5-0.5B	Zero-Shot	5.7	22.6	49.9	93.7	3.2	9.0	-
	FFT	58.3 \pm 0.28	33.3 \pm 0.37	86.1 \pm 0.46	1253.0 \pm 10.2	58.9 \pm 0.25	48.2 \pm 0.23	0.90
	LoRA	55.6 \pm 0.28	32.0 \pm 0.35	86.9 \pm 0.45	1206.0 \pm 10.1	58.6 \pm 0.22	45.5 \pm 0.24	0.65
	QLoRA	53.8 \pm 0.36	30.1 \pm 0.41	85.2 \pm 0.47	1178.4 \pm 10.2	56.9 \pm 0.27	46.7 \pm 0.39	0.88
	LoRA-One	56.0 \pm 0.25	29.9 \pm 0.32	87.0 \pm 0.49	1208.4 \pm 9.5	57.2 \pm 0.20	45.5 \pm 0.23	0.88
	Uni-LoRA	52.5 \pm 0.21	32.0 \pm 0.34	86.0 \pm 0.46	1227.3 \pm 10.9	58.0 \pm 0.29	42.4 \pm 0.39	0.69
	S-MFT Attn(Ours)	57.9 \pm 0.27	33.2 \pm 0.31	86.6 \pm 0.47	1243.0 \pm 8.2	59.6 \pm 0.20	47.8 \pm 0.37	0.61 2.92
TinyLlama-1.1B	S-MFT MLP (Ours)	59.0 \pm 0.21	33.4 \pm 0.32	87.3 \pm 0.45	1306.0 \pm 8.4	60.0 \pm 0.17	48.9 \pm 0.39	0.62 3.13
	S-MFT Both(Ours)	59.5 \pm 0.22	34.8 \pm 0.34	87.0 \pm 0.48	1349.3 \pm 8.6	59.2 \pm 0.19	49.4 \pm 0.38	0.67
	Zero-Shot	1.0	26.1	49.8	211.8	4.0	6.8	-
	FFT	57.3 \pm 0.33	30.4 \pm 0.34	85.8 \pm 0.44	1180.9 \pm 9.2	60.3 \pm 0.27	47.9 \pm 0.23	0.93
Gemma-2B	LoRA	57.5 \pm 0.41	30.4 \pm 0.22	86.9 \pm 0.47	1167.6 \pm 9.5	58.2 \pm 0.19	47.9 \pm 0.27	0.77
	QLoRA	55.9 \pm 0.35	26.2 \pm 0.35	81.5 \pm 0.48	1142.8 \pm 11.5	56.5 \pm 0.22	46.2 \pm 0.38	0.62
	LoRA-One	57.2 \pm 0.30	29.4 \pm 0.31	87.2 \pm 0.48	1170.5 \pm 8.9	59.5 \pm 0.21	46.2 \pm 0.24	0.66
	Uni-LoRA	55.4 \pm 0.27	27.1 \pm 0.28	84.5 \pm 0.44	1122.0 \pm 11.8	54.7 \pm 0.14	44.4 \pm 0.22	0.63
	S-MFT Attn(Ours)	56.8 \pm 0.20	30.4 \pm 0.29	87.3 \pm 0.47	1170.9 \pm 7.4	60.4 \pm 0.15	49.1 \pm 0.37	0.61 2.98
	S-MFT MLP (Ours)	57.4 \pm 0.30	30.9 \pm 0.20	87.7 \pm 0.48	1237.9 \pm 8.2	62.6 \pm 0.16	47.4 \pm 0.35	0.60 3.65
	S-MFT Both(Ours)	57.6 \pm 0.22	32.0 \pm 0.32	87.4 \pm 0.47	1188.0 \pm 7.7	61.0 \pm 0.19	48.7 \pm 0.39	0.74
Phi-2.27B	Zero-Shot	2.6	26.4	56.6	586.2	2.8	5.6	-
	FFT	60.9 \pm 0.37	31.3 \pm 0.35	86.4 \pm 0.44	1339.0 \pm 10.8	60.5 \pm 0.27	50.7 \pm 0.26	0.88
	LoRA	58.3 \pm 0.32	29.6 \pm 0.30	86.2 \pm 0.46	1178.0 \pm 9.7	57.4 \pm 0.20	48.0 \pm 0.23	0.64
	QLoRA	56.7 \pm 0.36	29.9 \pm 0.39	85.1 \pm 0.46	1152.3 \pm 10.4	55.8 \pm 0.25	46.1 \pm 0.33	0.63
	LoRA-One	58.4 \pm 0.32	30.1 \pm 0.32	86.0 \pm 0.46	1224.7 \pm 10.4	58.4 \pm 0.22	49.5 \pm 0.25	0.70
	Uni-LoRA	56.6 \pm 0.29	30.4 \pm 0.32	83.5 \pm 0.43	1194.7 \pm 10.9	57.4 \pm 0.20	49.9 \pm 0.25	0.71
	S-MFT Attn (Ours)	60.5 \pm 0.24	31.2 \pm 0.30	87.4 \pm 0.45	1348.8 \pm 8.6	63.5 \pm 0.24	50.3 \pm 0.21	0.53 7.21
Phi-2.27B	S-MFT MLP (Ours)	61.4 \pm 0.26	31.9 \pm 0.31	87.4 \pm 0.47	1402.6 \pm 9.8	62.4 \pm 0.22	51.1 \pm 0.21	0.57 8.06
	S-MFT Both (Ours)	61.6 \pm 0.25	31.9 \pm 0.28	87.6 \pm 0.49	1361.8 \pm 9.1	60.2 \pm 0.20	52.3 \pm 0.22	0.58
	Zero-Shot	2.3	25.7	50.1	87.4	9.8	1.5	-
	FFT	60.5 \pm 0.37	38.2 \pm 0.32	86.4 \pm 0.45	1413.9 \pm 9.6	71.9 \pm 0.29	56.5 \pm 0.22	0.86
Phi-2.27B	LoRA	59.8 \pm 0.34	37.1 \pm 0.22	88.1 \pm 0.49	1382.3 \pm 9.7	71.1 \pm 0.20	53.7 \pm 0.25	0.67
	QLoRA	58.3 \pm 0.39	33.9 \pm 0.28	85.7 \pm 0.47	1354.6 \pm 10.3	69.4 \pm 0.28	56.9 \pm 0.37	0.72
	LoRA-One	60.1 \pm 0.34	35.9 \pm 0.20	85.4 \pm 0.45	1380.7 \pm 9.7	69.6 \pm 0.27	53.0 \pm 0.24	0.60
	Uni-LoRA	59.0 \pm 0.33	35.0 \pm 0.39	86.5 \pm 0.47	1370.6 \pm 9.6	70.3 \pm 0.28	58.0 \pm 0.31	0.72
	S-MFT Attn(Ours)	60.3 \pm 0.24	37.8 \pm 0.27	88.0 \pm 0.45	1403.9 \pm 9.3	72.4 \pm 0.20	56.1 \pm 0.25	0.46 5.21
	S-MFT MLP (Ours)	61.4 \pm 0.25	38.6 \pm 0.25	87.7 \pm 0.47	1468.3 \pm 9.1	71.7 \pm 0.23	58.8 \pm 0.31	0.54 7.33
	S-MFT Both(Ours)	61.9 \pm 0.26	39.1 \pm 0.28	88.5 \pm 0.45	1414.5 \pm 9.0	72.4 \pm 0.21	57.2 \pm 0.28	0.64

Baselines & Datasets. We fully follow the experimental settings of LLaVA-v1.5 [29] and TinyLLaVA [69], which serve as our strong FFT baselines. Specifically, we use the same training data as in their setups and evaluate our models across multiple downstream tasks, including GQA [2], MMMU [58], POPE [27], MME [15], SQA [38], and TextVQA [47]. In addition to FFT, we also compare MFT against several representative PEFT approaches, such as LoRA [21], QLoRA [8], LoRA-One [65], and Uni-LoRA [25], to demonstrate its effectiveness and efficiency.

4.2. Main Reseults

We implement our key MFT extension S-MFT, which provides greater flexibility and optimization stability, as the primary experimental setting, and conduct extensive ablation studies to demonstrate its effectiveness, efficiency, and overall advantages over other fine-tuning methods. We also implement Hard Mask Fine-Tuning (H-MFT) in our experiments as a comparison to Soft Mask Fine-Tuning (S-MFT).

Comparison. Tab. 1 contains our main experiment results of S-MFT, which achieves strong and consistent performance across all four backbones and six evaluation tasks. All the experiments follow TinyLLaVA [69] settings to train one epoch with SigLIP [59] as the vision tower. We implement three S-MFT variants: 1) S-MFT Attn, 2) S-MFT MLP, and 3) S-MFT Both, which we apply learnable masks to the attention weights, MLP weights, or both within Transformer [56] blocks. The Epoch and the Time show the training iterations and the time cost of each method to achieve the best performance. Compared with FFT and four mainstream PEFT methods, S-MFT yields notable gains on most benchmarks while requiring significantly fewer training iterations and time. Among S-MFT variants, applying masks to both attention and MLP layers consistently delivers the highest overall accuracy, whereas module-specific masking (Attn or MLP) achieves similar results with slightly reduced computational cost. These results collectively demonstrate that S-MFT provides a robust, effective, and efficient fine-tuning alterna-

Table 2. Comparison between Soft Mask Fine-Tuning (S-MFT) and Hard Mask Fine-Tuning (H-MFT) on Qwen2.5-0.5B and TinyLLaMA-1.1B. The sparsity levels for H-MFT are selected based on the value distribution of the learned soft masks.

Method	GQA \uparrow	POPE \uparrow	SQA-Image \uparrow	TextVQA \uparrow
Qwen2.5-0.5B				
S-MFT	59.0	87.2	59.5	48.8
S-MFT STE	59.1	87.1	59.5	48.6
H-MFT 0.01%	56.1	85.9	57.9	43.9
H-MFT 0.05%	59.1	86.6	59.4	48.0
H-MFT 0.1%	53.0	85.3	57.9	44.8
TinyLlama-1.1B				
S-MFT	57.8	86.8	60.7	48.4
S-MFT STE	57.7	87.0	59.4	48.2
H-MFT 0.5%	56.2	86.7	54.9	43.1
H-MFT 1.0%	57.5	86.9	59.5	48.2
H-MFT 1.5%	51.2	84.1	57.1	46.2

tive that retains or exceeds full-tuning performance across diverse VLM architectures and downstream tasks.

H-MFT & S-MFT. We further analyze the impact of different gradient computation strategies and the relationship between S-MFT and H-MFT on two small language model backbones, as summarized in Tab. 2. For the soft variant, we compare S-MFT, which uses the true derivative of the sigmoid, and S-MFT (STE), which applies the straight-through estimator for gradient flow. Across both backbones, S-MFT and S-MFT (STE) achieve nearly identical performance, confirming that S-MFT optimization is insensitive to the gradient formulation and stable under both training dynamics. We then construct H-MFT using the sparsity levels inferred from the learned soft mask distributions shown in Sec. 5. The results show that H-MFT with sparsity similar to that learned by S-MFT achieves performance closest to S-MFT, while more aggressive pruning or denser masking results in noticeable degradation. These findings suggest that the continuous masks learned by S-MFT can not only optimize model performance but also reveal meaningful and interpretable sparse connectivity patterns.

4.3. Ablation Studies

Different Vision Tower. Since all our primary experiments follow the default setting of TinyLLaVA [69] using SigLIP [59] as the vision tower, we want to validate the generality of S-MFT on more vision tower backbones. Tab.3 shows the results of our exploration using CLIP-ViT-Large [46] as the vision tower of Qwen2.5-0.5B and TinyLLaMA-1.1B language models. The results indicate that S-MFT can also achieve better performance than FFT and LoRA across different vision tower backbones, supporting its generality.

Scale Up Study. To verify the scalability of our approach, we extend S-MFT to larger Qwen and LLaMA architectures, including Qwen2.5-7B, LLaMA2-7B [52] and Vicuna-

Table 3. Ablation studies of different vision tower backbones of Qwen2.5-0.5B and TinyLlama-1.1B language model backbones.

Method	GQA \uparrow	POPE \uparrow	SQA-Image \uparrow	TextVQA \uparrow
Qwen2.5-0.5B + CLIP-ViT-Large				
FFT	55.7	85.3	57.6	44.2
LoRA	55.1	85.2	57.5	43.7
S-MFT	56.5	85.8	57.9	44.7
TinyLlama-1.1B + CLIP-ViT-Large				
FFT	58.0	85.5	59.9	46.3
LoRA	57.8	85.4	59.3	45.9
S-MFT	58.7	86.0	60.5	46.9
Qwen2.5-7B + SigLIP-ViT-Large				
FFT	64.7	87.7	76.4	64.0
LoRA	63.9	86.8	74.5	63.7
S-MFT	64.9	87.7	78.1	64.2
LLaMA2-7B + CLIP-ViT-Large				
FFT	61.7	87.2	68.8	57.7
LoRA	61.9	87.6	68.3	56.5
S-MFT	62.2	87.8	69.0	57.6
Vicuna-7B + CLIP-ViT-Large				
FFT	62.6	88.1	69.5	58.4
LoRA	62.4	88.3	69.7	58.3
S-MFT	63.2	88.0	70.3	58.8

7B [68], as summarized in Tab. 4. All mask parameters, including initialization and temperature, are directly estimated from the corresponding smaller models without additional tuning. Despite this zero-shot transfer of hyperparameters, S-MFT continues to outperform or match FFT and LoRA across all tasks. These findings indicate that S-MFT generalizes well across model scales and that the learned masking behavior remains consistent and effective in larger architectures, further validating that S-MFT is a scalable fine-tuning paradigm suitable for large-scale foundation models.

Initialization Value & Temperature. As discussed in Sec. 3.2.2, our S-MFT primarily depends on two key hyperparameters, which are the initialization value of the score matrix and the temperature. Therefore, before conducting our main experiments, we expect a comprehensive understanding of each backbone’s behavior under combinations of initialization values and temperatures. We perform an ablation study on the combinations of these two hyperparam-

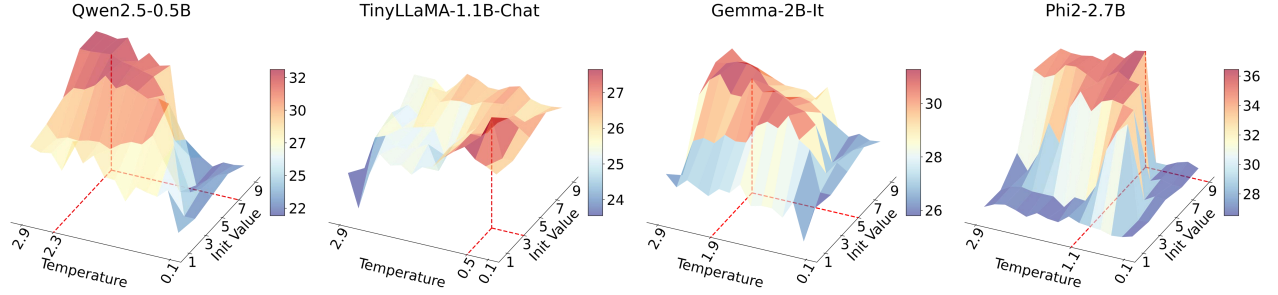


Figure 3. Ablation study on the initialization value of the score matrix and temperature across four language backbones. Each surface plot illustrates the performance variation of MMMU benchmark of Soft Mask Fine-Tuning (S-MFT) under different hyperparameter combinations. The red dashed line in each plot marks the optimal configuration for the corresponding backbone.

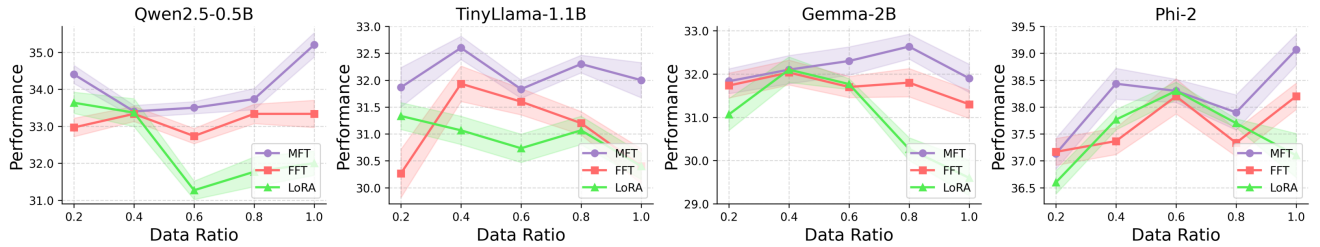


Figure 4. Performance comparison of S-MFT, FFT, and LoRA under varying training data proportions across four VLM backbones. Each curve shows the performance with standard deviation of the MMMU benchmark as the proportion of training data increases. S-MFT consistently maintains strong performance across most data proportions, showing robustness regardless of data scale.

eters for each of the four language backbones, summarizing in Fig. 3. We use 10% of the training data and the normal gradient formulation for this ablation study to gain quick intuition and a sanity check, and observe that each backbone exhibits its own high-performance region in the initialization-temperature space. It is also worth noting that within the same model, even identical ratios of the initialization value to the temperature do not yield comparable performance. These optimal regions are well-shaped and consistently higher than their surroundings, forming smooth, stable plateaus rather than fluctuating landscapes, indicating that S-MFT is robust to hyperparameter variations. We adopt the best configuration from this ablation study as the default setting for our subsequent full-dataset experiments. Concretely, we use (initialization-temperature) values of 7.0-2.3, 3.0-0.5, 5.0-1.3, and 9.0-1.1 for Qwen2.5-0.5B, TinyLLaMA-1.1B, Gemma-2B, and Phi-2-2.7B, respectively.

Data Proportion Ablation. We further investigate the data efficiency of S-MFT by varying the proportion of training data used during fine-tuning, as illustrated in Fig. 4. For Qwen and Gemma, S-MFT consistently achieves higher overall performance than FFT and LoRA, particularly at higher data proportions, indicating the scalability of S-MFT as the dataset size increases on these two backbones. In contrast, results of TinyLLaMA exhibit relatively larger per-

formance fluctuations in S-MFT, but it still maintains a slight edge in most settings. The results of Phi-2 show greater variability, with S-MFT outperforming other methods at both low and high data ratios, suggesting better adaptability to changes in data scale. Overall, while the absolute trend varies by backbone, S-MFT generally demonstrates more stable or higher performance across data scales, reflecting its stable effectiveness.

Layer-wise Ablation. We conduct a layer-wise sensitivity study to examine how different layers respond to the application of soft masks. As shown in Fig. 5, masking different layer ranges yields notably different adaptation effects. For both Qwen2.5-0.5B and TinyLLaMA-1.1B, mid-level layers (e.g., layers 8–11) produce the highest average performance, approaching the results of full-layer training. In contrast, masking only shallow or deep layers leads to larger performance drops, suggesting that early layers capture modality alignment features that should remain stable, while deeper layers are less adaptable once the representational space becomes highly specialized. These findings indicate that S-MFT primarily benefits from mid-layer reconfiguration, where representational flexibility remains high, offering insights for future layer selection and efficient partial-adaptation strategies.

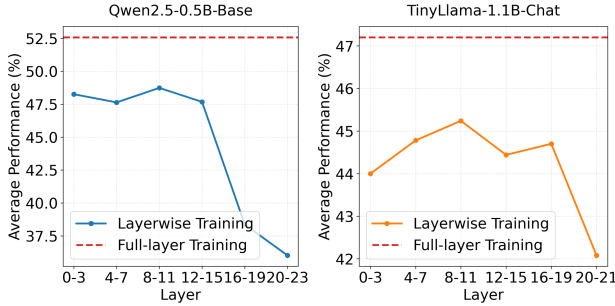


Figure 5. Layer-wise analysis of S-MFT on Qwen2.5-0.5B and TinyLlama-1.1B. Each curve shows the average performance when masks are applied only to a subset of layers, compared with full-layer training (red dashed line).

5. Analysis

Figure 6 presents the proportions of near-zero mask values in the mask learned by S-MFT across different projection types in attention and MLP for two model families, Qwen2.5 and LLaMA2, with multiple model scales. A clear and consistent trend can be observed across both series.

Within the Qwen2.5 family, the overall pattern shows that attention projections exhibit substantially higher proportions of near-zero masks than MLP projections, suggesting that Qwen2.5 models inherently contain more redundancy within their attention layers than in their MLP layers. This observation indicates a potential architectural characteristic of the Qwen2.5 family that its expressivity and adaptability are concentrated mainly in the attention module, where multiple heads may encode overlapping contextual dependencies. Moreover, as the model size increases, the overall proportions of near-zero values decrease, implying that larger Qwen2.5 models make more effective use of their representational capacity, leading to more balanced and efficient parameter utilization. Among the attention projections, the K projection consistently shows the most significant proportion of near-zero masks, suggesting that Key representations exhibit greater overlap or redundancy that S-MFT can safely remove. The Q projection follows a similar but less pronounced trend, while the V and O projections display much smaller proportions that gradually vanish as model size grows. This phenomenon implies that the value and output projections in larger Qwen2.5 models become increasingly essential, leading to little redundancy, and reflecting a progressive specialization of attention components as model scaling up.

In contrast, the LLaMA2 series exhibits a distinct sparsity pattern. Overall, from a model-level perspective, the LLaMA2 family exhibits a significantly higher proportion of near-zero mask values compared to the Qwen2.5 family. The attention projections in LLaMA2 family still have higher proportions of near-zero mask values than the MLP

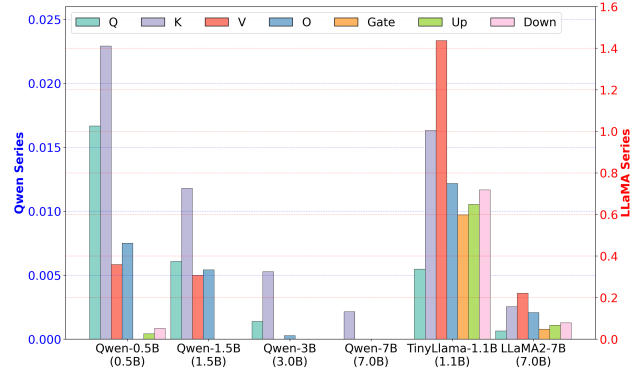


Figure 6. The Proportion of near-zero mask values learned by S-MFT across different model architectures and sizes. We compare the proportion of near-zero mask values across two model families, Qwen2.5 and LLaMA2. Each bar corresponds to a projection type within the attention and MLP in the model. The left y-axis denotes Qwen2.5 models, and the right y-axis denotes LLaMA models.

projections, indicating that redundancy in LLaMA models remains primarily within the attention layers. But the MLP layers have noticeably higher proportions of near-zero mask values than the Qwen2.5 family, suggesting that LLaMA2 family distributes redundancy more evenly across both attention and MLP modules, reflecting a more intertwined functional structure between the two. Within the attention module in LLaMA2 family, the V projection consistently has the highest proportion of near-zero masks, followed by K and O, while the Q projection shows the least redundancy. This pattern implies that the Value in LLaMA2 plays a less selective role in large-scale representations, with more overlap across heads, whereas Query representations remain highly task-specific and information-critical. For the MLP layers, the near-zero mask proportions of Gate, Up, and Down projections are relatively balanced, suggesting that LLaMA’s MLP module does not exhibit a single dominant redundancy source. Moreover, as the model size increases, none of the projections’ near-zero proportions vanish entirely in LLaMA2 family. This observation indicates that, compared with Qwen2.5 family, LLaMA2 family exhibits greater persistent redundancy, which may stem from architectural differences that favor representational overlap and broader parameter utilization.

6. Conclusion

In this paper, we rethink fine-tuning for VLMs from a structural reparameterization perspective grounded in MFT. In addition to the recently proven effective Hard Mask Fine-Tuning (H-MFT), we introduce Soft Mask Fine-Tuning (S-MFT) as an extension, and apply both to the VLMs. We redefine model adaptation as a process of structural reparameterization rather than weight modification. Experiments demonstrate that our S-MFT is an effective, efficient, and

robust fine-tuning paradigm that consistently surpasses mainstream PEFT methods and even FFT, while requiring fewer training iterations.

Limitations. Due to computational and time constraints, our experiments primarily focus on small backbones. While the experiments reveal clear trends and stable mechanisms, the full potential of MFT on larger backbones, as well as more model architectures, remains unexplored. In future work, we plan to extend MFT to larger backbones and more complex multimodal reasoning benchmarks, aiming to establish a comprehensive methodology.

Rethinking Fine-Tuning: Unlocking Hidden Capabilities in Vision-Language Models

Supplementary Material

7. Implementation Details

Our experiments are conducted on a server equipped with 4 NVIDIA A100 GPUs with 80GB of memory. We borrow the code of LLaVA [30] and TinyLLaVA [69], as well as their LLaVA-v1.5-Mix-665K instruction dataset for projector pre-training and the BLIP-Laion-CC-SBU-558K instruction dataset for fine-tuning. We also use the official evaluation protocols in both codebases for all our evaluation experiments.

8. Experiments

8.1. Learning Rate Ablation

Since our Soft Mask Fine-Tuning (S-MFT) starts from mask values that are initialized to be as close to 1 as possible

$$W \odot M_{\text{init}} \approx W \odot I = W, \quad (12)$$

where W is the original pre-trained weight, M_{init} is the initialized mask, and I represents the identity matrix. For such near-identity masks, we conduct extensive experiments and find that using a small learning rate often leads to gradients that become nearly zero or even vanish during training. Therefore, we perform a learning rate ablation study and identify the range in which the learning rate actually has an effect, as visualized in Fig. 7. In this ablation study, we use the optimal combination of initialization value and temperature for each language model backbone with 10% training data. Results on the MMMU benchmark indicate that the model learns effectively only when the learning rate is approximately 0.1. Our main experiments also follow this ablation study, using the optimal learning rate identified for each language model backbone.

8.2. Mask Analysis

Here, we present additional analyses of the learned masks for Gemma-2B and Phi-2-2.7B. As shown in the Fig. 8, Gemma-2B exhibits noticeably higher near-zero ratios in several attention projections, particularly K and V, indicating stronger redundancy within its attention subsystem. In contrast, Phi-2-2.7B shows consistently low near-zero ratios across all mappings, suggesting a more uniformly utilized and less redundant architecture.

8.3. Results of H-MFT and S-MFT

In the main paper, we compare H-MFT and S-MFT across two language model backbones, Qwen2.5-0.5B and

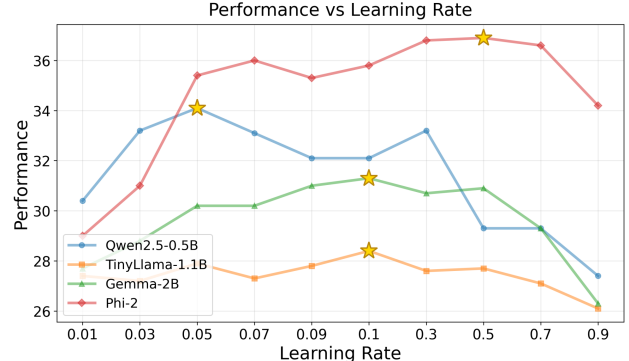


Figure 7. Performance of four language backbones on the MMMU benchmark across different learning rates.

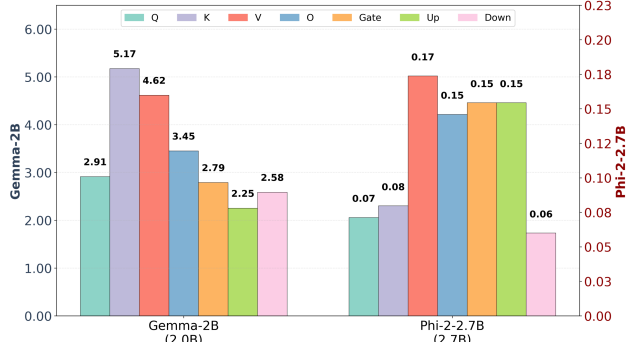


Figure 8. Learned mask distributions for Gemma-2B and Phi-2-2.7B.

TinyLLaMA-1.1B. Due to space limitations, only four of the six evaluation tasks used in our main table are shown. Here, we present the whole table and further supplement the results with H-MFT and S-MFT performance on two additional language-model backbones, Gemma-2B and Phi-2-2.7B, as shown in Tab. 5.

8.4. Results of Vision Towers

We supplement the results of the other two small language model backbones, Gemma-2B and Phi-2-2.7B, with CLIP in Tab. 6.

8.5. Scale Up Results

We supplement the results from two additional large language model backbones, Qwen2.5-14B and LLaMA2-13B, in Tab. 7 to demonstrate the scalability of our S-MFT method.

Table 5. Comparison between Soft Mask Fine-Tuning (S-MFT) and Hard Mask Fine-Tuning (H-MFT) on four small language model backbones. The sparsity levels for H-MFT are selected based on the distribution of values in the learned soft masks.

Method	GQA \uparrow	MMMU \uparrow	POPE \uparrow	MME \uparrow	SQA-Image \uparrow	TextVQA \uparrow
Qwen2.5-0.5B						
S-MFT	59.0	34.6	87.2	1342.1	59.5	48.8
S-MFT STE	59.1	34.9	87.1	1357.1	59.5	48.6
H-MFT 0.01%	56.1	31.7	85.9	1302.1	57.9	43.9
H-MFT 0.05%	59.1	33.8	86.6	1345.7	59.4	48.0
H-MFT 0.1%	53.0	31.4	85.3	1212.4	57.9	44.8
TinyLLaMA-1.1B						
S-MFT	57.8	32.3	86.8	1196.1	60.7	48.4
S-MFT STE	57.7	32.0	87.0	1189.1	59.4	48.2
H-MFT 0.5%	56.2	28.1	86.7	1174.7	54.9	43.1
H-MFT 1.0%	57.5	31.6	86.9	1191.9	59.5	48.2
H-MFT 1.5%	51.2	28.2	84.1	1112.4	57.1	46.2
Gemma2-2B						
S-MFT	61.4	32.1	87.1	1362.7	60.4	52.0
S-MFT STE	61.7	31.9	87.7	1356.9	59.6	52.8
H-MFT 1%	55.1	31.4	85.9	1272.3	59.0	47.2
H-MFT 3%	56.5	31.8	86.1	1301.5	60.5	51.4
H-MFT 5%	55.4	30.7	85.5	1242.1	60.0	48.9
Phi-2-2.7B						
S-MFT	62.1	38.8	88.0	1423.5	72.6	57.0
S-MFT STE	63.3	38.4	88.1	1428.7	72.4	57.0
H-MFT 0.05%	61.1	37.1	87.3	1393.3	71.0	56.7
H-MFT 0.1%	62.1	38.4	87.7	1427.0	72.1	56.6
H-MFT 0.3%	60.7	35.9	86.8	1345.6	69.8	55.4

Table 6. Ablation studies of different vision tower backbones across four small language model backbones.

Method	GQA \uparrow	MMMU \uparrow	POPE \uparrow	MME \uparrow	SQA-Image \uparrow	TextVQA \uparrow
Qwen2.5-0.5B + CLIP-ViT-Large						
FFT	55.7	34.2	85.3	1197.9	57.6	44.2
LoRA	55.1	32.7	85.2	1196.7	57.5	43.7
S-MFT	56.5	34.9	85.8	1208.4	57.9	44.7
TinyLlama-1.1B + CLIP-ViT-Large						
FFT	58.0	27.9	85.5	1284.6	59.9	46.3
LoRA	57.8	27.5	85.4	1278.4	59.3	45.9
S-MFT	58.7	28.7	86.0	1289.0	60.5	46.9
Gemma-2B + CLIP-ViT-Large						
FFT	56.4	32.3	84.4	1194.1	60.0	45.8
LoRA	57.2	28.4	83.9	1249.7	57.6	45.9
S-MFT	58.4	33.1	85.8	1254.4	60.8	46.0
Phi-2-2.7B + CLIP-ViT-Large						
FFT	59.4	36.3	86.8	1448.6	71.2	53.4
LoRA	58.7	35.8	86.6	1437.1	70.9	53.3
S-MFT	60.3	37.0	87.9	1467.9	72.1	55.0

Table 7. Scaling study of MFT on larger Qwen and LLaMA VLMs. We evaluate S-MFT on Qwen2.5-14B and LLaMA2-13B, comparing it with FFT and LoRA, using hyperparameters transferred from the smaller backbone analysis.

Method	GQA \uparrow	POPE \uparrow	SQA-Image \uparrow	TextVQA \uparrow
Qwen2.5-14B + SigLIP-ViT-Large				
FFT	65.6	88.5	80.1	66.1
LoRA	65.3	87.8	79.1	66.0
S-MFT	66.5	88.4	80.4	67.0
LLaMA2-13B + CLIP-ViT-Large				
FFT	61.7	87.2	68.8	57.7
LoRA	61.9	87.6	68.3	56.5
S-MFT	62.2	87.8	69.0	57.6

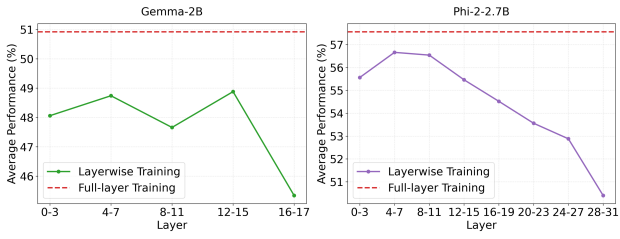


Figure 9. Layerwise ablation study for Gemma-2B and Phi-2.7B.

8.6. Layerwise Analysis

We supplement the layerwise ablation study of the other two small language model backbones in Fig. 9. Overall, for Gemma-2B and Phi-2.7B, the most sensitive layers remain in the middle of the model. A little difference here is that, for Gemma, the sensitive layers are located near both ends of the model’s middle region, whereas for Phi, they appear earlier in the network. This reveals that, although S-MFT generally benefits from the middle layers across different model architectures, the exact locations of sensitivity vary across architectures.

8.7. Theoretical Guarantee Supplement

For our case, to theoretically support that S-MFT has better optimization potential than FFT, we need to verify that $\Delta_{\text{train}} + \Delta_{\text{complexity}} < 0$.

For the first term, we first supplement a set of exemplar training loss statistics in Tab. 8. It shows the mean training loss once training stabilizes, indicating that S-MFT can further reduce it relative to FFT.

Then, we can ensure the first term $\Delta_{\text{train}} < 0$.

For the second term, we need to compare the encoded model complexity. Given d as the total number of weights, z as the weights suppressed by the learned mask (i.e., mask values close to zero), and b as the bit width. Since our S-MFT

Table 8. Exemplar training loss statistics of different language model backbones after training is stable.

Language Model Backbone	FFT	S-MFT
Qwen2.5-0.5B	1.0414	0.9731
TinyLLaMA-1.1B	0.9145	0.8822
Gemma-2B	0.9368	0.9021
Phi-2.2.7B	0.9499	0.9049

operates at weight-level masking granularity, we have

$$C(h_{\text{FFT}}) \approx bd, \quad C(h_{\text{S-MFT}}) \approx b(1-p)d + \log_2 \binom{d}{z}, \quad (13)$$

where $p = z/d$ represents the effective sparsity induced by the learned mask. The first term of $C_{\text{S-MFT}}$ corresponds to the cost of storing the active (non-suppressed) weights, while the second term captures the index cost of identifying suppressed connections. Further, we have $\log_2 \binom{d}{z} \approx dH(p)$, where

$$H(p) = -p \log_2 p - (1-p) \log_2 (1-p). \quad (14)$$

Then, the second term can be described as

$$\Delta_{\text{complexity}} = C(h_{\text{S-MFT}}) - C(h_{\text{FFT}}) \approx d[H(p) - bp]. \quad (15)$$

For practice, we always use $b = 8$ or 16 . Our S-MFT does not explicitly impose sparsity. However, across all backbones, it consistently converges to an emergent sparsity of approximately 1%–3% in the language model and connector modules. To illustrate a representative case, we set $b = 8$ and $p = 0.03$ in the calculation shown below.

$$H(p) - bp = H(0.03) - 8 \cdot 0.03 \approx -0.046 < 0. \quad (16)$$

Then, we have the second term $\Delta_{\text{complexity}} < 0$.

Combining both the first and second terms, we have

$$U(h_{\text{S-MFT}}) - U(h_{\text{FFT}}) = \Delta_{\text{train}} + \Delta_{\text{complexity}} < 0. \quad (17)$$

Finally, we conclude that $U(h_{\text{S-MFT}}) < U(h_{\text{FFT}})$, which means the MFT can further reduce the test loss upper bound compared with FFT and theoretically support our proposed method.

8.8. Trainable Parameter Ratio

Table 9 compares the ratio of trainable parameters under different MFT configurations across the four language model backbones. This table demonstrates that: (1) MFT-Attn configuration is highly parameter efficient, requiring only 7–30% of the full parameters. The ratio of the trainable parameters of MFT-Attn is even less than that of LoRA on some language model backbones; (2) MFT-MLP provides

a mid-cost alternative still substantially cheaper than FFT; and (3) MFT-Both offers a balanced choice that preserves the best performance while remaining significantly more efficient than full fine-tuning.

Table 9. The comparison of the trainable parameter ratio of different methods.

Method	Trainable	Ratio
Qwen2.5-0.5B Total Params: 495869568		
FFT	495869568	1.00
LoRA	72222464	0.15
MFT Attn	45875200	0.09
MFT MLP	315621376	0.64
MFT Both	359661568	0.73
TinyLLaMA-1.1B Total Params: 1106606080		
FFT	1106606080	1.00
LoRA	107483136	0.10
MFT Attn	214171648	0.19
MFT MLP	767819776	0.69
MFT Both	975437824	0.88
Gemma-2B Total Params: 2512730112		
FFT	2512730112	1.00
LoRA	163450880	0.07
MFT Attn	176422912	0.07
MFT MLP	1818492928	0.72
MFT Both	1988362240	0.79
Phi-2-2.7B Total Params: 2789191680		
FFT	2789191680	1.00
LoRA	198251520	0.07
MFT Attn	848363520	0.30
MFT MLP	1687224320	0.60
MFT Both	2526085120	0.91

References

- [1] Aishwarya Agrawal, Jiasen Lu, Stanislaw Antol, Margaret Mitchell, C. Lawrence Zitnick, Dhruv Batra, and Devi Parikh. Vqa: Visual question answering, 2016. 1
- [2] Joshua Ainslie, James Lee-Thorp, Michiel de Jong, Yury Zemlyanskiy, Federico Lebrón, and Sumit Sanghai. Gqa: Training generalized multi-query transformer models from multi-head checkpoints, 2023. 5
- [3] Sanjeev Arora, Rong Ge, Behnam Neyshabur, and Yi Zhang. Stronger generalization bounds for deep nets via a compression approach. In *International conference on machine learning*, 2018. 4
- [4] Jinze Bai, Shuai Bai, Yunfei Chu, Zeyu Cui, Kai Dang, Xiaodong Deng, Yang Fan, Wenbin Ge, Yu Han, Fei Huang, et al. Qwen technical report. *arXiv preprint arXiv:2309.16609*, 2023. 1
- [5] Yue Bai, Huan Wang, ZHIQIANG TAO, Kunpeng Li, and Yun Fu. Dual lottery ticket hypothesis. In *International Conference on Learning Representations*, 2022. 2
- [6] Yoshua Bengio, Nicholas Léonard, and Aaron Courville. Estimating or propagating gradients through stochastic neurons for conditional computation, 2013. 3
- [7] Florian Bordes, Richard Yuanzhe Pang, Anurag Ajay, Alexander C Li, Adrien Bardes, Suzanne Petryk, Oscar Mañas, Zhiqiu Lin, Anas Mahmoud, Bargav Jayaraman, et al. An introduction to vision-language modeling. *arXiv preprint arXiv:2405.17247*, 2024. 1
- [8] Tim Dettmers, Artidoro Pagnoni, Ari Holtzman, and Luke Zettlemoyer. Qlora: Efficient finetuning of quantized llms, 2023. 2, 5
- [9] Jacob Devlin, Ming-Wei Chang, Kenton Lee, and Kristina Toutanova. BERT: Pre-training of deep bidirectional transformers for language understanding. In *Proceedings of the 2019 Conference of the North American Chapter of the Association for Computational Linguistics: Human Language Technologies, Volume 1 (Long and Short Papers)*, pages 4171–4186. Association for Computational Linguistics, 2019. 1
- [10] Gongfan Fang, Xinyin Ma, and Xinchao Wang. Structural pruning for diffusion models. In *Advances in Neural Information Processing Systems*, pages 16716–16728. Curran Associates, Inc., 2023. 2
- [11] Gongfan Fang, Xinyin Tan Ma, Michael Bi Mi, and Xinchao Wang. Isomorphic pruning for vision models. *arXiv preprint arXiv:2407.04616*, 2024. 2
- [12] Gongfan Fang, Hongxu Yin, Saurav Muralidharan, Greg Heinrich, Jeff Pool, Jan Kautz, Pavlo Molchanov, and Xinchao Wang. Maskllm: Learnable semi-structured sparsity for large language models. *arXiv preprint arXiv:2409.17481*, 2024. 3
- [13] Jonathan Frankle and Michael Carbin. The lottery ticket hypothesis: Finding sparse, trainable neural networks, 2019. 2
- [14] Elias Frantar and Dan Alistarh. SparseGPT: Massive language models can be accurately pruned in one-shot. *arXiv preprint arXiv:2301.00774*, 2023. 3
- [15] Chaoyou Fu, Peixian Chen, Yunhang Shen, Yulei Qin, Meng-dan Zhang, Xu Lin, Jinrui Yang, Xiawu Zheng, Ke Li, Xing Sun, Yunsheng Wu, Rongrong Ji, Caifeng Shan, and Ran

He. Mme: A comprehensive evaluation benchmark for multi-modal large language models, 2025. 5

[16] Suriya Gunasekar, Yi Zhang, Jyoti Aneja, Caio César Teodoro Mendes, Allie Del Giorno, Sivakanth Gopi, Mojan Javaheripi, Piero Kauffmann, Gustavo de Rosa, Olli Saarikivi, et al. Textbooks are all you need. *arXiv preprint arXiv:2306.11644*, 2023. 1, 4

[17] Song Han, Xingyu Liu, Huizi Mao, Jing Pu, Ardavan Pedram, Mark A. Horowitz, and William J. Dally. Eie: efficient inference engine on compressed deep neural network. In *Proceedings of the 43rd International Symposium on Computer Architecture*, page 243–254. IEEE Press, 2016. 2

[18] Song Han, Huizi Mao, and William J. Dally. Deep compression: Compressing deep neural networks with pruning, trained quantization and huffman coding, 2016. 2

[19] Bairu Hou, Qibin Chen, Jianyu Wang, Guoli Yin, Chong Wang, Nan Du, Ruoming Pang, Shiyu Chang, and Tao Lei. Instruction-following pruning for large language models, 2025. 3

[20] Neil Houlsby, Andrei Giurgiu, Stanislaw Jastrzebski, Bruna Morrone, Quentin De Laroussilhe, Andrea Gesmundo, Mona Attariyan, and Sylvain Gelly. Parameter-efficient transfer learning for NLP. In *Proceedings of the 36th International Conference on Machine Learning*, 2019. 2

[21] Edward J. Hu, Yelong Shen, Phillip Wallis, Zeyuan Allen-Zhu, Yuanzhi Li, Shean Wang, Lu Wang, and Weizhu Chen. Lora: Low-rank adaptation of large language models, 2021. 2, 5

[22] Forrest N. Iandola, Song Han, Matthew W. Moskewicz, Khalid Ashraf, William J. Dally, and Kurt Keutzer. SqueezeNet: Alexnet-level accuracy with 50x fewer parameters and ~ 0.5 mb model size, 2016. 2

[23] Dawid J. Kopczko, Tijmen Blankevoort, and Yuki M. Asano. Vera: Vector-based random matrix adaptation, 2024. 2

[24] Brian Lester, Rami Al-Rfou, and Noah Constant. The power of scale for parameter-efficient prompt tuning. In *Proceedings of the 2021 Conference on Empirical Methods in Natural Language Processing*, pages 3045–3059. Association for Computational Linguistics, 2021. 2

[25] Kaiyang Li, Shaobo Han, Qing Su, Wei Li, Zhipeng Cai, and Shihao Ji. Uni-lora: One vector is all you need. In *The 39th Conference on Neural Information Processing Systems (NeurIPS)*, 2025. 2, 5

[26] Xiang Lisa Li and Percy Liang. Prefix-tuning: Optimizing continuous prompts for generation, 2021. 2

[27] Yifan Li, Yifan Du, Kun Zhou, Jinpeng Wang, Wayne Xin Zhao, and Ji-Rong Wen. Evaluating object hallucination in large vision-language models. In *The 2023 Conference on Empirical Methods in Natural Language Processing*, 2023. 5

[28] Zongxia Li, Xiyang Wu, Hongyang Du, Fuxiao Liu, Huy Nghiêm, and Guangyao Shi. A survey of state of the art large vision language models: Alignment, benchmark, evaluations and challenges, 2025. 1

[29] Haotian Liu, Chunyuan Li, Yuheng Li, and Yong Jae Lee. Improved baselines with visual instruction tuning, 2023. 5

[30] Haotian Liu, Chunyuan Li, Qingyang Wu, and Yong Jae Lee. Visual instruction tuning, 2023. 1, 4, 10

[31] Hongyi Liu, Rajarshi Saha, Zhen Jia, Youngsuk Park, Ji-aji Huang, Shoham Sabach, Yu-Xiang Wang, and George Karypis. Proxsparse: Regularized learning of semi-structured sparsity masks for pretrained llms. *arXiv preprint arXiv:2502.00258*, 2025. 3

[32] Shih-Yang Liu, Chien-Yi Wang, Hongxu Yin, Pavlo Molchanov, Yu-Chiang Frank Wang, Kwang-Ting Cheng, and Min-Hung Chen. Dora: Weight-decomposed low-rank adaptation, 2024. 2

[33] Xiao Liu, Kaixuan Ji, Yicheng Fu, Weng Tam, Zhengxiao Du, Zhilin Yang, and Jie Tang. P-tuning: Prompt tuning can be comparable to fine-tuning across scales and tasks. In *Proceedings of the 60th Annual Meeting of the Association for Computational Linguistics (Volume 2: Short Papers)*, pages 61–68. Association for Computational Linguistics, 2022. 2

[34] Yuanxin Liu, Fandong Meng, Zheng Lin, Peng Fu, Yanan Cao, Weiping Wang, and Jie Zhou. Learning to win lottery tickets in BERT transfer via task-agnostic mask training. In *Proceedings of the 2022 Conference of the North American Chapter of the Association for Computational Linguistics: Human Language Technologies*, pages 5840–5857. Association for Computational Linguistics, 2022. 2

[35] Yiheng Liu, Junhao Ning, Sichen Xia, Xiaohui Gao, Ning Qiang, Bao Ge, Junwei Han, and Xintao Hu. Pruning large language models by identifying and preserving functional networks. *arXiv preprint arXiv:2508.05239*, 2025. 2

[36] Yuchen Liu, Yaoming Wang, Bowen Shi, Xiaopeng Zhang, Wenrui Dai, Chenglin Li, Hongkai Xiong, and Qi Tian. Meteor: Multi-encoder collaborative token pruning for efficient vision language models, 2025. 2

[37] Zhuang Liu, Mingjie Sun, Tinghui Zhou, Gao Huang, and Trevor Darrell. Rethinking the value of network pruning. In *ICLR*, 2019. 2

[38] Pan Lu, Swaroop Mishra, Tony Xia, Liang Qiu, Kai-Wei Chang, Song-Chun Zhu, Oyvind Tafjord, Peter Clark, and Ashwin Kalyan. Learn to explain: Multimodal reasoning via thought chains for science question answering. In *The 36th Conference on Neural Information Processing Systems (NeurIPS)*, 2022. 5

[39] Xinyin Ma, Gongfan Fang, and Xinchao Wang. Llm-pruner: On the structural pruning of large language models. In *Advances in Neural Information Processing Systems*, pages 21702–21720. Curran Associates, Inc., 2023. 2

[40] David A McAllester. Some pac-bayesian theorems. In *Proceedings of the eleventh annual conference on Computational learning theory*, 1998. 4

[41] Pavlo Molchanov, Stephen Tyree, Tero Karras, Timo Aila, and Jan Kautz. Pruning convolutional neural networks for resource efficient inference, 2017. 2

[42] Changdae Oh, Hyesu Lim, Mijoo Kim, Dongyoon Han, Sangdoo Yun, Jaegul Choo, Alexander Hauptmann, Zhi-Qi Cheng, and Kyungwoo Song. Towards calibrated robust fine-tuning of vision-language models, 2024. 2

[43] Long Ouyang, Jeff Wu, Xu Jiang, Diogo Almeida, Carroll L. Wainwright, Pamela Mishkin, Chong Zhang, Sandhini Agarwal, Katarina Slama, Alex Ray, John Schulman, Jacob Hilton, Fraser Kelton, Luke Miller, Maddie Simens, Amanda Askell,

Peter Welinder, Paul Christiano, Jan Leike, and Ryan Lowe. Training language models to follow instructions with human feedback, 2022. 1

[44] Tan-Hanh Pham and Chris Ngo. Rarl: Improving medical vlm reasoning and generalization with reinforcement learning and lora under data and hardware constraints, 2025. 1

[45] Qwen, :, An Yang, Baosong Yang, Beichen Zhang, Binyuan Hui, Bo Zheng, Bowen Yu, Chengyuan Li, Dayiheng Liu, Fei Huang, Haoran Wei, Huan Lin, Jian Yang, Jianhong Tu, Jianwei Zhang, Jianxin Yang, Jiaxi Yang, Jingren Zhou, Junyang Lin, Kai Dang, Keming Lu, Keqin Bao, Kexin Yang, Le Yu, Mei Li, Mingfeng Xue, Pei Zhang, Qin Zhu, Rui Men, Runji Lin, Tianhao Li, Tianyi Tang, Tingyu Xia, Xingzhang Ren, Xuancheng Ren, Yang Fan, Yang Su, Yichang Zhang, Yu Wan, Yuqiong Liu, Zeyu Cui, Zhenru Zhang, and Zihan Qiu. Qwen2.5 technical report, 2025. 4

[46] Alec Radford, Jong Wook Kim, Chris Hallacy, Aditya Ramesh, Gabriel Goh, Sandhini Agarwal, Girish Sastry, Amanda Askell, Pamela Mishkin, Jack Clark, Gretchen Krueger, and Ilya Sutskever. Learning transferable visual models from natural language supervision, 2021. 1, 3, 4, 6

[47] Amanpreet Singh, Vivek Natarjan, Meet Shah, Yu Jiang, Xinlei Chen, Devi Parikh, and Marcus Rohrbach. Towards vqa models that can read. In *Proceedings of the IEEE Conference on Computer Vision and Pattern Recognition*, pages 8317–8326, 2019. 5

[48] Mingjie Sun, Zhuang Liu, Anna Bair, and J. Zico Kolter. A simple and effective pruning approach for large language models, 2024. 3

[49] Chaofan Tao, Lu Hou, Haoli Bai, Jiansheng Wei, Xin Jiang, Qun Liu, Ping Luo, and Ngai Wong. Structured pruning for efficient generative pre-trained language models. In *Findings of the Association for Computational Linguistics: ACL 2023*, pages 10880–10895. Association for Computational Linguistics, 2023. 3

[50] Gemma Team, Thomas Mesnard, Cassidy Hardin, Robert Dadashi, Surya Bhupatiraju, Shreya Pathak, Laurent Sifre, Morgane Rivière, Mihir Sanjay Kale, Juliette Love, et al. Gemma: Open models based on gemini research and technology. *arXiv preprint arXiv:2403.08295*, 2024. 1, 4

[51] Hugo Touvron, Thibaut Lavril, Gautier Izacard, Xavier Martinet, Marie-Anne Lachaux, Timothée Lacroix, Baptiste Rozière, Naman Goyal, Eric Hambro, Faisal Azhar, Aurelien Rodriguez, Armand Joulin, Edouard Grave, and Guillaume Lample. Llama: Open and efficient foundation language models, 2023. 1

[52] Hugo Touvron, Louis Martin, Kevin Stone, Peter Albert, Amjad Almahairi, Yasmine Babaei, Nikolay Bashlykov, Soumya Batra, Prajjwal Bhargava, Shruti Bhosale, et al. Llama 2: Open foundation and fine-tuned chat models. *arXiv preprint arXiv:2307.09288*, 2023. 6

[53] Huan Wang and Yun Fu. Trainability preserving neural pruning. In *ICLR*, 2023. 2

[54] Huan Wang, Can Qin, Yulun Zhang, and Yun Fu. Neural pruning via growing regularization. In *International Conference on Learning Representations (ICLR)*, 2021. 2

[55] Huan Wang, Can Qin, Yue Bai, Yulun Zhang, and Yun Fu. Recent advances on neural network pruning at initialization, 2022. 2

[56] Thomas Wolf, Lysandre Debut, Victor Sanh, Julien Chaumond, Clement Delangue, Anthony Moi, Pierrick Cistac, Tim Rault, Rémi Louf, Morgan Funtowicz, Joe Davison, Sam Shleifer, Patrick von Platen, Clara Ma, Yacine Jernite, Julien Plu, Canwen Xu, Teven Le Scao, Sylvain Gugger, Mariama Drame, Quentin Lhoest, and Alexander M. Rush. Transformers: State-of-the-art natural language processing. In *Proceedings of the 2020 Conference on Empirical Methods in Natural Language Processing: System Demonstrations*, pages 38–45. Association for Computational Linguistics, 2020. 5

[57] Yi Xu, Yuxin Hu, Zaiwei Zhang, Gregory P. Meyer, Siva Karthik Mustikovela, Siddhartha Srinivasa, Eric M. Wolff, and Xin Huang. Vlm-ad: End-to-end autonomous driving through vision-language model supervision, 2025. 1

[58] Xiang Yue, Yuansheng Ni, Kai Zhang, Tianyu Zheng, Ruqi Liu, Ge Zhang, Samuel Stevens, Dongfu Jiang, Weiming Ren, Yuxuan Sun, Cong Wei, Botao Yu, Ruibin Yuan, Renliang Sun, Ming Yin, Boyuan Zheng, Zhenzhu Yang, Yibo Liu, Wenhao Huang, Huan Sun, Yu Su, and Wenhui Chen. Mmmu: A massive multi-discipline multimodal understanding and reasoning benchmark for expert agi. In *Proceedings of CVPR*, 2024. 5

[59] Xiaohua Zhai, Basil Mustafa, Alexander Kolesnikov, and Lucas Beyer. Sigmoid loss for language image pre-training, 2023. 1, 4, 5, 6

[60] Yuexiang Zhai, Hao Bai, Zipeng Lin, Jiayi Pan, Shengbang Tong, Yifei Zhou, Alane Suhr, Saining Xie, Yann LeCun, Yi Ma, and Sergey Levine. Fine-tuning large vision-language models as decision-making agents via reinforcement learning. In *The Thirty-eighth Annual Conference on Neural Information Processing Systems*, 2024. 2

[61] Dan Zhang, Tao Feng, Lilong Xue, Yuandong Wang, Yuxiao Dong, and Jie Tang. Parameter-efficient fine-tuning for foundation models, 2025. 1, 2

[62] Mingyuan Zhang, Yue Bai, Huan Wang, Yizhou Wang, Qihua Dong, and Yun Fu. Boosting large language models with mask fine-tuning, 2025. 2, 3

[63] Peiyuan Zhang, Guangtao Zeng, Tianduo Wang, and Wei Lu. Tinyllama: An open-source small language model, 2024. 4

[64] Qingru Zhang, Minshuo Chen, Alexander Bukharin, Nikos Karampatziakis, Pengcheng He, Yu Cheng, Weizhu Chen, and Tuo Zhao. Adalora: Adaptive budget allocation for parameter-efficient fine-tuning, 2023. 2

[65] Yuanhe Zhang, Fanghui Liu, and Yudong Chen. Lora-one: One-step full gradient could suffice for fine-tuning large language models, provably and efficiently, 2025. 2, 5

[66] Mengjie Zhao, Tao Lin, Fei Mi, Martin Jaggi, and Hinrich Schütze. Masking as an efficient alternative to finetuning for pretrained language models. In *Proceedings of the 2020 Conference on Empirical Methods in Natural Language Processing (EMNLP)*, pages 2226–2241. Association for Computational Linguistics, 2020. 3

[67] Kecheng Zheng, Wei Wu, Ruili Feng, Kai Zhu, Jiawei Liu, Deli Zhao, Zheng-Jun Zha, Wei Chen, and Yujun Shen. Regularized mask tuning: Uncovering hidden knowledge in pre-trained vision-language models. In *ICCV*, 2023. 3

- [68] Lianmin Zheng, Wei-Lin Chiang, Ying Sheng, Siyuan Zhuang, Zhanghao Wu, Yonghao Zhuang, Zi Lin, Zhuohan Li, Dacheng Li, Eric. P Xing, Hao Zhang, Joseph E. Gonzalez, and Ion Stoica. Judging llm-as-a-judge with mt-bench and chatbot arena, 2023. [1](#), [6](#)
- [69] Baichuan Zhou, Ying Hu, Xi Weng, Junlong Jia, Jie Luo, Xien Liu, Ji Wu, and Lei Huang. Tinyllava: A framework of small-scale large multimodal models, 2024. [4](#), [5](#), [6](#), [10](#)